

Wire-Arc Additive Manufacturing – Forging Process Chain Simulation Analysis of Aluminium Alloy



N. Musa^{1,2}, M. S. Adenan^{1,2*}, J. Saedon², Y. HP. Manurung^{1,2}, M. F. Mat^{1,2}

¹Smart Manufacturing Research Institute, Universiti Teknologi MARA, 40450, Shah Alam, Selangor, Malaysia.

²School of Mechanical Engineering, College of Engineering, Universiti Teknologi MARA, 40450, Shah Alam, Selangor, Malaysia



ABSTRACT: This research models an efficient process chain for combining wire-arc additive manufacturing (WAAM) and forging operations to evaluate process properties and identify the optimal strategy for minimizing stress and displacement, ensuring dimensional accuracy in thin-wall component. Simufact.Welding software was used to simulate the WAAM process for Al 6061 and ER 5356, examining various fixture strategies, substrate thicknesses, heat inputs, and electrical parameters. The simulations revealed that singular heat input along with dual fixtures led to reduced distortion and displacement. The geometry resulting from WAAM was imported into Simufact.Forging to test five different press stroke strategies. It was found that single press strokes with 2 mm reduction showed the minimum effective plastic strain, and maximum with 6 mm reduction. Multi-press strokes, although showing similar performance, were preferred for their ability to reduce impact loads and improve material properties, with effective plastic strain and stress ranging from 0.01 to 0.09 and 0.86 to 32.90 MPa, respectively. The simulations accurately predicted deformation and residual stress, confirming that Case A using 25.4 mm substrate thickness and 2 clamping with single heat input is the optimal strategy for minimizing distortion and stress while maintaining process efficiency.

KEYWORDS: Wire arc additive manufacturing (WAAM), welding simulation, forging simulation, process chain simulation, aluminium alloy.

[Received Oct. 22, 2024; Revised Jan. 9, 2025; Accepted Feb. 2, 2025]

Print ISSN: 0189-9546 | Online ISSN: 2437-2110

I. INTRODUCTION

Direct energy deposition (DED) is a process in which a thermal source is used to melt the material during the deposition (Hafenecker et al., 2023). The most widely applied DED process is wire-arc additive manufacturing (WAAM) due to its high deposition rates and cost-competitive compared to frequently used DED (Köhler et al., 2019). According to ASTM F2792-12a, WAAM defined as the combination of an electric arc utilized as heat source and wire as the deposited or feedstock material (Rodrigues et al., 2019). In addition, WAAM technology has increasingly been applied in industrial manufacturing due to its capability to produce meter-sized metallic components with high material utilization (Maurya et al., 2022). WAAM processes typically produce coarse microstructures with columnar grains that vary with deposition strategy. For 5356 aluminum alloy, the effect of different process parameters (e.g., heat input, travel speed, and wire feed rate) on the grain size, texture, and homogeneity of the deposited material remains insufficiently understood.

Studies reported that solidification WAAM of aluminium alloy presented a major challenge because of the thermomechanical cycles occurring during WAAM and the creation of undesirable microstructure featuring large

columnar grains (Altıparmak et al., 2021). High strength aluminium alloy such as 2xxx and 7xxx series alloys have difficulty processing due to solidification-related issues resulting from thermochemical cycles that occur during the WAAM process (Altıparmak et al., 2021). The mechanical properties of 2024 aluminium alloy are related to the pore behaviour due to higher number of cavities on the deposited surface. A higher number of porosities affect the optimal performance of tensile strength of WAAM interlayer specifically the transverse mechanical properties compared the longitudinal direction (Fu et al., 2021). Furthermore, the WAAM process of 6xxx series alloy observed crack-free microstructures for Al 6061 (Altıparmak et al., 2021). The intermetallic compound in 6061 aluminium alloy generally well-controlled during heat treatment, hence, making it eligible for high deposition rate process in WAAM structural applications (Doumenc et al., 2022). In recent years, Al-Mg alloy, 5356 aluminium alloy is often used in locomotive carriages, chemical pressure vessels, ships, aviation and other industries because of its good weldability and corrosion resistance (Jiangang et al., 2022). However, Wang et al., (2023) showed the increasing deposition height in WAAM AA5356 increase the average grain size and porosities deformation due to temperature rise and local thermal cycling,

*Corresponding author: mshahriman@uitm.edu.my

leading to nuclei grow in all directions in depositing a new layer. Recent studies found that the temperature gradient and cooling rate of the molten pool influence the growth grain size in the microstructure and mechanical properties of aluminium alloy on cold metal transfer (CMT) (Li et al., 2020). Wide solidification such as the temperature range between solidus and liquidus temperature of aluminium most likely leads to smooth cracks (Köhler et al., 2019). Additionally, Arana et al. (2021) noted that multiple layers in the WAAM process contribute to the growth of pores due to the heat input of new layer formation.

Hybrid manufacturing in combining additive manufacturing (AM) and forming operations attracted much attention in terms of the manufacturing process chain and provided a good relationship for these processes to overcome WAAM limitations (Li et al., 2021). On the other hand, a combination of AM and metal forming promises to reduce manufacturing time and cost per part besides overcome the limitations of AM such as metallurgical defects, rough surfaces, low productivity and low geometrical accuracy (Hafenecker et al., 2023). Hybrid manufacturing is a designation of different additive manufacturing and subtractive processes to overcome limitations of a process (Pragana et al., 2021). The combinations of AM with metal forming aim to improve the shape of the deposited material layers by local plastic deformation while providing higher stiffness and wear resistance to the build parts (Pragana et al., 2021). According to the study on hybrid manufacturing by metal forming and WAAM, hybrid parts show good metallurgical bonding in the transition zone (Bambach et al., 2020). Limited understanding of how the WAAM process affects the microstructure of 5356 aluminium alloy, especially when subsequently subjected to forging. This includes how the deposition pattern, layer orientation, and residual stresses influence grain structure, dendritic formation, and precipitation phases.

To apply the hybrid method, optimum process parameters should be utilized to investigate the accurate prediction and deformation during the processes. Since hybrid manufacturing involves a combination of different technologies, optimization process parameters may require two different simulations. Research on optimizing the DED process typically analysed distortions and residual stress during the WAAM process. R. Israr et al (Israr et al., 2020) conducted a study on different fixations strategies during the WAAM process by finite element analysis with the software LS-DYNA to enhance the geometrical accuracy of the substrate. The study on the optimization of hybrid manufacturing process combining forging and WAAM, analysed the processing maps of ANN model predictions, revealing the hybrid processing route as the most promising for part production due to the good agreement between experimental flow stress and coefficient values (Maurya et al., 2022). However, the biological system of ANN does not provide an overview of the deformation of actual components but relies solely on the parameters. Rajesh et al. (2021) used Simufact.Forming to evaluate the finite element comparative analysis of the multi-step forming process of hot closed die forging process. The research found the outcomes

of effective stress, effective plastic strain, and temperature distribution during the forging process. This software has the capability to improve geometry deformation during process chain of multi-forged process. In a recent study on forming-welding process chain, experimental comparison between weld bead size, distortion, and residual stress revealed good agreement with percentage error below 12% for bead size while 0.35 mm for distortion of low carbon steel (Bauer et al., 2019). The numerical simulation analysis of forming and welding process predicts the major properties of the actual process parameters.

One of the main challenges in hybrid manufacturing is integrating the parameters of both WAAM and forging processes to achieve optimal results. This study to understand the interaction between WAAM and forging conditions (temperature, residual stress, strain rates) affect the final properties of 5356 aluminum. For instance, determining how to effectively control the transition from the additive deposition phase to the forging process to minimize defects like residual stresses and distortion is critical. Therefore, the paper is structured in two main simulation processes for WAAM by using Simufact.Welding and forging process chain by Simufact.Forging software to optimize the deformation of 5356 and 6061 aluminium alloy to establish a relationship between the input parameters and response variables. Simufact.Welding evaluates the distortion of WAAM geometry and residual stress, while SF analyses the effective plastic strain and stress distribution after the forging process. This paper simulates an efficient process-chained hybrid WAAM and forging operation to study the process properties, ensuring that the strategy with the least stress and minimum displacement guarantees the dimensional accuracy of the thin wall.

II. METHODOLOGY

The numerical analysis of wire-arc additive manufacturing (WAAM) to predict the optimal combination of welding parameters by analysing the distribution of distortion, residual stress, and effective plastic strain was carried out. This analysis involved defining material properties, welding parameters and the WAAM path line. Figure 1 illustrates the process chain simulation of WAAM and forging, which consists of three steps: geometric modelling, WAAM simulation, and forging simulation. Geometric modelling and FEM meshing performed using MSC Marc Mentat software. As part of the WAAM and forging process chain, the WAAM results served as the initial geometry for the forging simulation. The forging simulation included forming properties such as workpiece positioning and forging parameters. In this simulation, ER 5356 as the filler material for thin wall fabrication and Al 6061 as the substrate were employed. Material properties and chemical composition were extracted from the material library using Simufact software. Table 1 presents the chemical composition of the materials used that analysed by Hitachi EDX Quantax 70 Energy-X-ray Spectroscopy (EDX).

Table 1 Chemical composition (wt%) of material used in simulation

Alloy	ER 5356	Al 6061
Al	91.4	93.4
Si	0.3	0.1
Fe	0.4	0.2
Cu	1.1	0.3
Mn	0.3	0.1
Mg	5.6	5.0
Zn	-	0.2
Cr	0.6	0.7
Ti	0.3	-

As described in Table 2, a variety of scenarios (A to H) were analyzed to understand the effects of substrate thickness, heat input, and fixation strategy. These cases analyzed the interaction of the various parameters with distortion and residual stress during WAAM deposition. After WAAM deposition, forging was simulated to study the effects of different reduction lengths and types of press on the forging process. The cases (I to N) outlined in Table 3 illustrate the multi and single press variations in the forging sequence. The results of both WAAM and forging simulations were checked to evaluate the impact of different welding and forging parameters on the distortion, residual stress, and plastic strain and to determine the most productive process conditions for hybrid WAAM-forging.

Table 2 WAAM deposition cases

Case	Substrate thickness	Fixation strategies	Heat input
A	25.4 mm	2 clamps	Single
B			Multi
C		4 clamps	Single
D			Multi
E	38.1 mm	2 clamps	Single
F			Multi
G		4 clamps	Single
H			Multi

Table 3 Forging process cases

Case	Press	Reduction length, mm
I	Single press	2
J		4
K		6
L	Multi press	2
M		2, 2
N		2, 2, 2

The three-dimensional model of WAAM geometry in Simufact.Welding (SW) were developed to simulate bearing and clamping. MSC Marc Mentat FEM software modelled the wall and substrate before assigning in SW simulation. Figure 2 shows the construction of the wall dimensions of 110 mm (L) x 110 mm (H) x 15 mm (W). The robot follows 55 trajectories for all cases. The substrate, with thicknesses of 25.4 mm and 38.1 mm, has dimensions of 130 mm in length and 60 mm in width. Various fixture or clamp positions were studied using the same surface-to-surface contact, with all substrate corners constrained by different clamp shapes in the z-direction. Four cylindrical clamps and two cuboid clamps were the two types of fixtures modelled. Fixture positions were optimized based on the robot arm's movement during the actual welding process, as shown in Figure 3. The welding direction of alternate adjacent layers is reversed, with a cooling time of approximately 2 seconds and a 2 mm offset established for each layer to enhance heat dissipation within the model. Goldak's double ellipsoid model uses the parameters listed in Table 4 for the heat source in the welding simulation. The welding properties used in SW are detailed in Table 5.

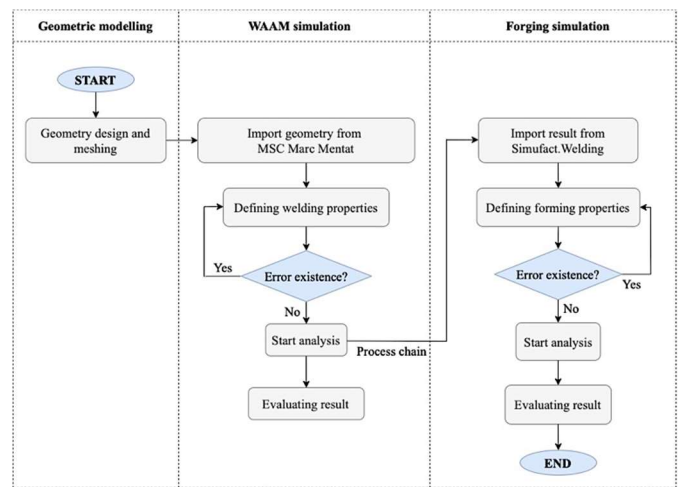


Figure 1 Process chain of simulation flow

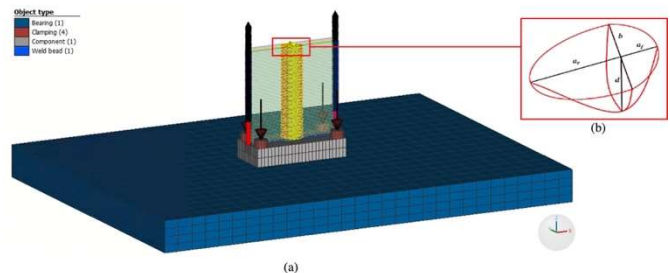


Figure 2 (a) WAAM geometry in SW; (b) Illustration model of Goldak filler aluminium (Napitupulu et al., 2020)

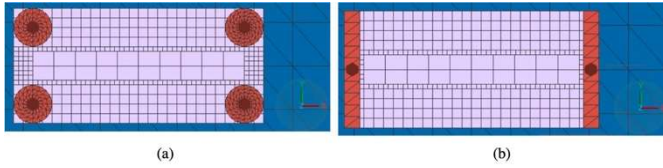


Figure 3 Fixture position; (a) Four cylindrical clamps; (b) Two cuboidal clamps

Table 4 Goldak’s heat source properties

Heat source properties	Value
Front length, a_f	5.0 mm
Rear length, a_r	12.0 mm
Width, b	8.0 mm
Depth, d	2.0 mm

Table 5 Welding properties in SW simulation

Welding properties	Parameter
Substrate thickness	25.4 – 38.1 mm
Fixation strategies	2 -4 clamps
Velocity	7 mm/s
Current	100 – 152 A
Voltage	13.2 – 15.2 V
Efficiency	0.8

Equations 1 and 2 describe the power densities during WAAM process. The local coordinates in Equation 1 defines heat flux in front section of heat source of the power density, $q_f(x, y, z)$ while Equation 2 defines the rear section of heat source, $q_r(x, y, z)$, during the WAAM process of double ellipsoid heat source modelling. The reconstructed model’s local coordinates are represented in the variable of x, y and z (Xian et al., 2022):

$$q_f(x, y, z) = \frac{6\sqrt{3}f_f Q}{a_f b c \pi \sqrt{\pi}} \cdot e^{-\frac{3x^2}{a_f^2}} \cdot e^{-\frac{3y^2}{b^2}} \cdot e^{-\frac{3z^2}{c^2}} \quad (1)$$

$$q_r(x, y, z) = \frac{6\sqrt{3}f_r Q}{a_r b c \pi \sqrt{\pi}} \cdot e^{-\frac{3x^2}{a_r^2}} \cdot e^{-\frac{3y^2}{b^2}} \cdot e^{-\frac{3z^2}{c^2}} \quad (2)$$

According to this model, $f_f + f_r = 2$ and Q represents the effective heat power [W] and is expressed as $Q = \eta \cdot U \cdot I$ where η, U and I denoting efficiency, welding voltage [V] and current [A], respectively. The variables a_f, a_r, b and c represents the length, width, depth of front and rear double ellipsoidal heat source parameters which define the shape of ellipses.

Modelling the heat source is crucial for the numerical simulation analysis of the welding process. The suitability of the heat source depends on the welding geometry and can be customized by the user. Thus, the double ellipsoidal model was implemented to simulate the real heat source of the GMAW process. This model is widely used for thermal simulation of moving heat sources in additive manufacturing. Figure 2(b)

shows the double ellipsoidal heat source model. The movement of the heat source during material deposition generates inconsistent energy distribution, defined as element nodes, in the form of heat flux density (Kiran et al., 2022).

B. Process Chain of Welding and Forging Simulation

The SW simulation output act as an initial condition of Simufact.Forging (SF) geometry and model properties. The study used this output as the initial geometry for the forging simulation model. Figure 4 shows the overall setup of the thin wall after the welding simulation, including the lower and upper dies. The WAAM and forging operations process chain utilizes a crank press, as applied in the actual experiment. The upper die pressing force is based on the library crank press in SF. This study incorporates Gurson's fracture damage criteria to establish failure criteria in the simulation, combining porosity evolution for the material (Mohamed et al., 2021). Table 6 presents the forging parameters assigned in SF for the WAAM and forging process chain, while Table 7 details the damage model parameters set up in SF. The simulation examines various press forces to investigate the stress effects of single and multi-press configurations, with press forces ranging from 2 mm, 4 mm, and 6 mm for single presses and a reduction of 2 mm for multi-presses.

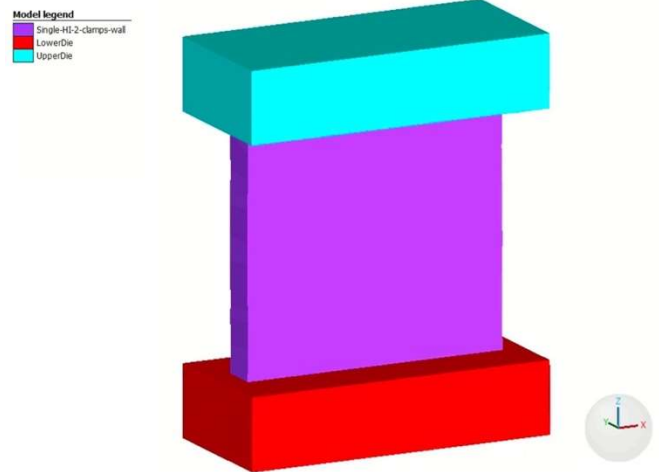


Figure 4 Forging geometry set up in Simufact.Forging

Table 6 Forging process parameters assigned in Simufact.Forging

Process Parameter	Properties / Value
Process type	Upsetting
Damage model	Gurson
Press	Crank press
	Crank radius: 70 mm
	Rod length: 30 mm
	Revolution: 100 rpm
Temperature	20°C
Stroke	2 mm, 4 mm, 6 mm

Table 7 The damage model parameters setup in Simufact.Forging

Constant	Parameter	Value
First yield Surface multiplier	q_1	1.5
Second yield multiplier	q_2	1.0
Initial void volume fraction	f_o	0.0
Critical void volume fraction	f_c	0.2
Failure void volume fraction	f_f	0.73
Volume fraction for void nucleation	f_n	0.04
Mean strain for nucleation	ε_n	0.3
Standard deviation	s_n	0.01

III. RESULTS AND DISCUSSION

A. Distortion and Residual Stress Distribution of Wire-arc Additive Manufacturing Model

The comparison of wire-arc additive manufacturing (WAAM) distortion is illustrated by the geometry model and total displacement in Simufact.Welding (SW). Table 8 presents the total displacement for each geometry, while Figure 5 shows the displacement distribution on the welding geometry. Case A, using 25.4 mm substrate thickness and 2 clamping with single heat input exhibits the minimum displacement changes compared to other cases, according to Table 8. Figure 5 reveals that Cases A, B, E, G, and H display similar displacement in the transversal direction welding zone, contrasting with the welding properties of other strategies. Substrate thickness does not show any apparent distortion in 55 layers of wall formation. Fixation strategies indicate that 2 cuboidal clamps result in low displacement compared to 4 cylindrical clamps for both substrate thicknesses. The results suggest that changing clamp orientation and types can reduce distortion. Rosli et al., (2021) demonstrated that edge fixation with 2 clamps is more effective in minimizing distortions compared to corner fixation with 4 clamps, as it reduces additional constraints on the substrate. Case G, which exhibits the highest displacement, concludes that transverse clamps are more effective than corner fixation. Therefore, transversal fixation plays a role in minimizing total distortion after the cooling process.

The thermal influences from the welding process mainly cause the distortion because the repeated cooling and heating, leading to higher stresses that deform welded walls (Gokul et al., 2022). Once the filler wire is heated, cooling slows down due to the time required for the heat to be transported throughout the molten pool and into the substrate. As the molten pool cools, it undergoes a liquid-to-solid phase transformation and releases latent heat during solidification (Ou et al., 2018). The cooling rate determines the weld metallurgical structure and heat affected zone (HAZ), which is affected by the heat input, wire feed rate, current and voltage (Rosli et al., 2021). The effective cooling time for 5356 aluminium alloy is 60 s (Wieczorowski et al., 2023). The wire feed rate is proportional to the current and voltage, so an increase in wire feed rate results in higher heat input. A single-heat input leads to high penetration and deposition, whereas multi-heat input alters the penetration and create more uniform straight wall (Greebmalai and Warinsiruk, 2020). In conclusion, the aim is to minimize the displacement changes

and reduce distortion of the substrate during the welding process by using a minimum number of clamps with a single heat input. Case A was selected as the primary geometry for process chain welding-forming in SF.

Table 8 Total displacement of different welding properties

Case	Substrate thickness	Fixation strategies	Heat input	Total displacement, mm	
				Min.	Max.
A	25.4 mm	2 clamps	Single	0.00	1.19
B			Multi	0.01	1.25
C	38.1 mm	4 clamps	Single	0.00	1.28
D			Multi	0.02	1.41
E	38.1 mm	2 clamps	Single	0.00	1.28
F			Multi	0.00	1.22
G	38.1 mm	4 clamps	Single	0.01	1.34
H			Multi	0.02	1.22

Table 9 presents the effective residual stresses in the substrate after the cooling process after the cooling process, while Figure 6 shows the colour distribution analysis. Case D exhibits the lowest residual stress distribution, while Case H shows the highest. The highest stress in Case D is due to the 4 cuboidal clamps on each edge of the substrate imposing extra constraints on the substrate surface (Israr et al., 2020). To ensure uniform process parameters and welding properties in the forging simulation, Case A is considered an optimal strategy for reducing residual stress distribution on the substrate and wall during the WAAM process. Case A shows acceptable and lower residual stress compared to other cases, making it the preferred choice for initial geometry in the process chain simulation. Future studies should investigate the accuracy of residual stress by specifying longitudinal and transverse stress values to better comprehend material strength properties, as the residual stress distribution in WAAM components remains unclear (Sun et al., 2021). Figure 9 summarizes the deformation and stress data for thin wall formation in the SW simulation.

Table 9 Equivalent stress of different welding properties

Case	Substrate thickness	Fixation strategies	Heat input	Equivalent stress, MPa	
				Min.	Max.
A	25.4 mm	2 clamps	Single	0.63	114.69
B			Multi	0.65	161.15
C	38.1 mm	4 clamps	Single	0.68	143.52
D			Multi	1.12	76.18
E	38.1 mm	2 clamps	Single	0.32	119.75
F			Multi	0.25	149.19
G	38.1 mm	4 clamps	Single	0.23	132.71
H			Multi	0.82	162.09

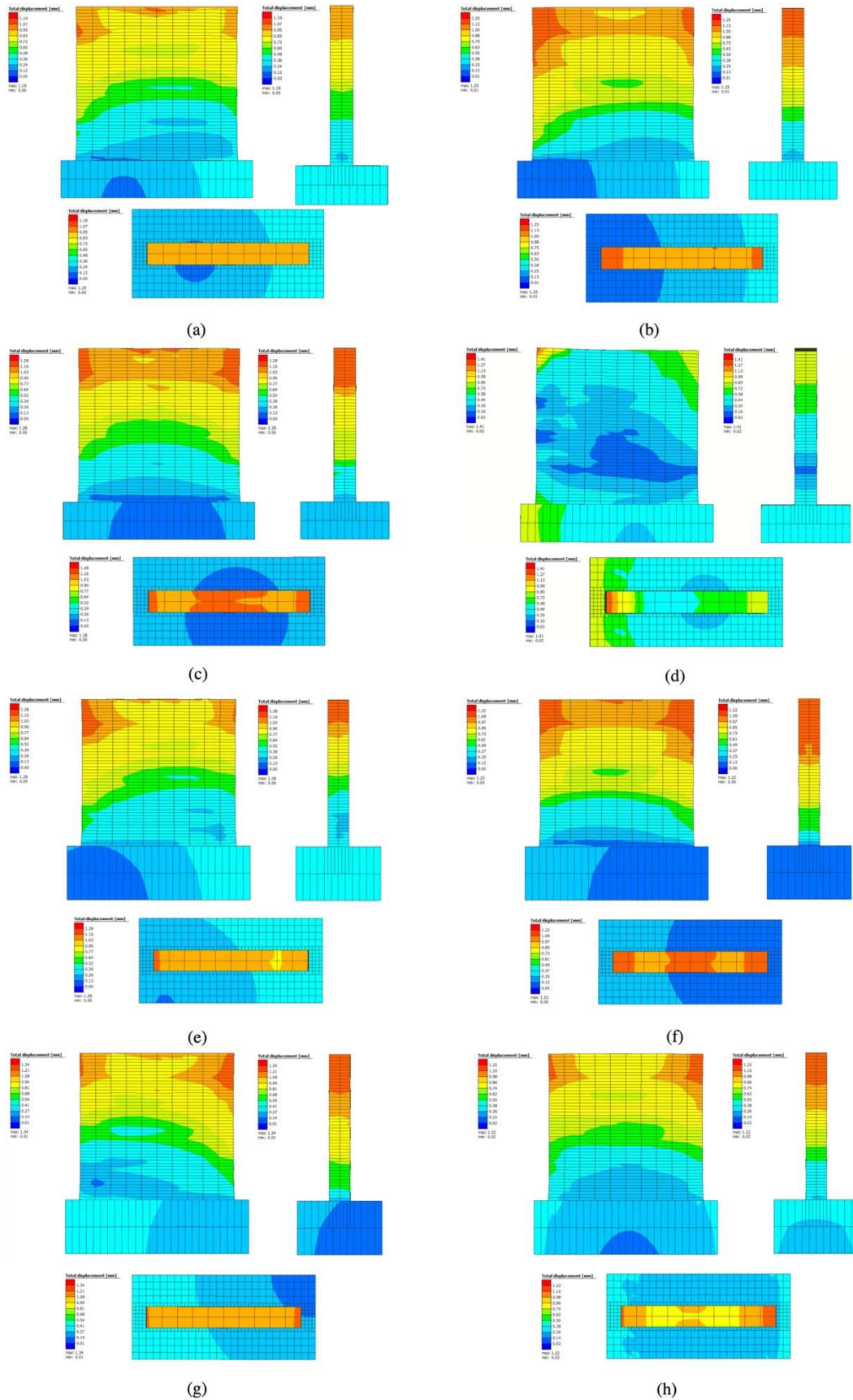


Figure 5 Total displacement of different welding properties; (a) Case A; (b) Case B; (c) Case C; (d) Case D; (e) Case E; (f) Case F; (g) Case G; (h) Case H

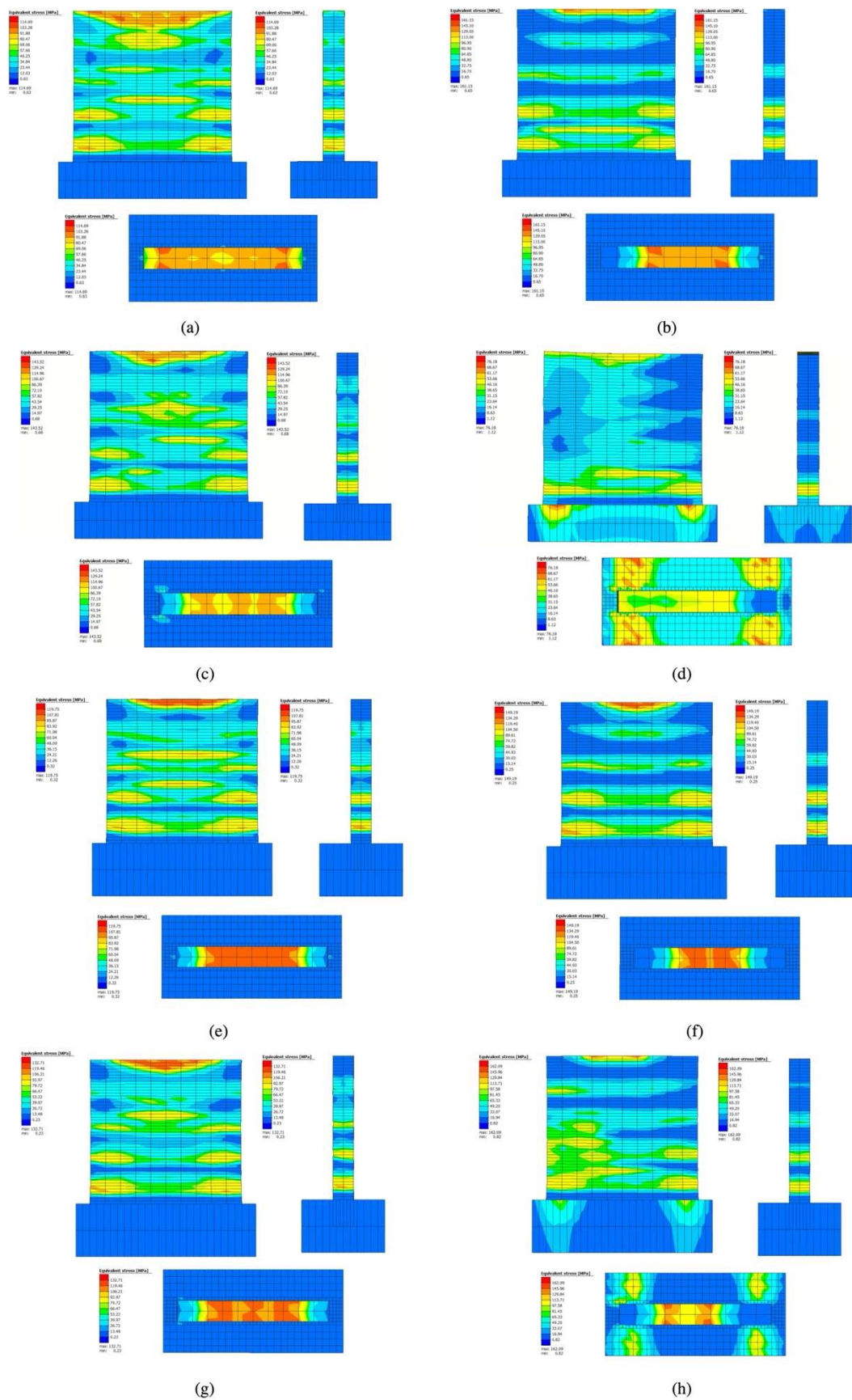


Figure 6 Equivalent stress of different welding properties; (a) Case A; (b) Case B; (c) Case C; (d) Case D; (e) Case E; (f) Case F; (g) Case G; (h) Case H

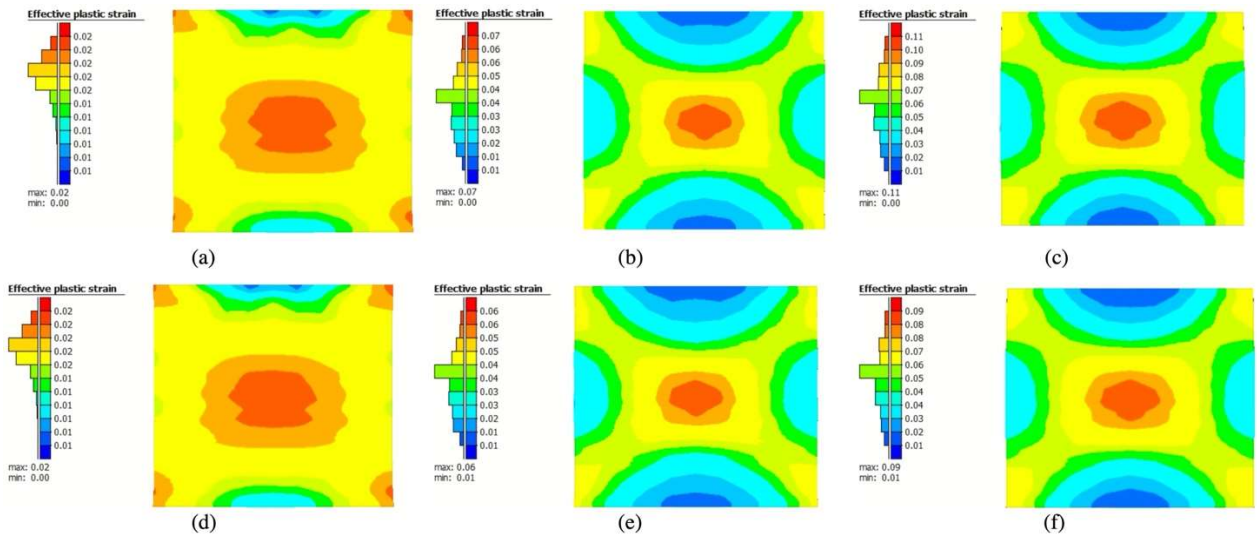


Figure 7 Effective plastic strain of different forging properties; (a) Case I; (b) Case J; (c) Case K; (d) Case L; (e) Case M; (f) Case N

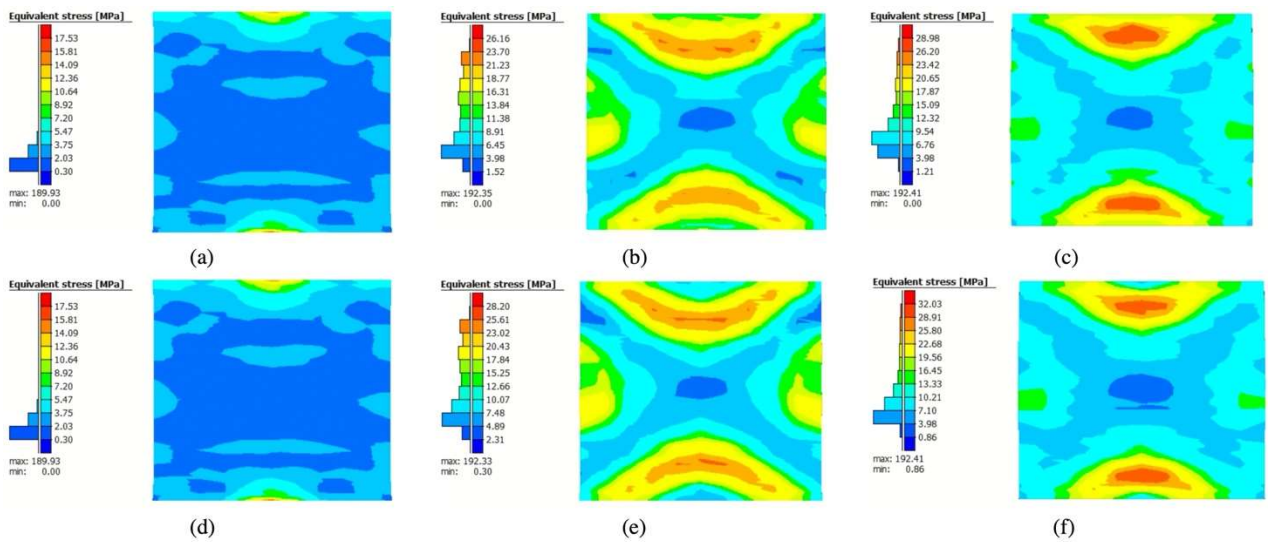


Figure 8 Equivalent stress of different forging properties; (a) Case I; (b) Case J; (c) Case K; (d) Case L; (e) Case M; (f) Case N

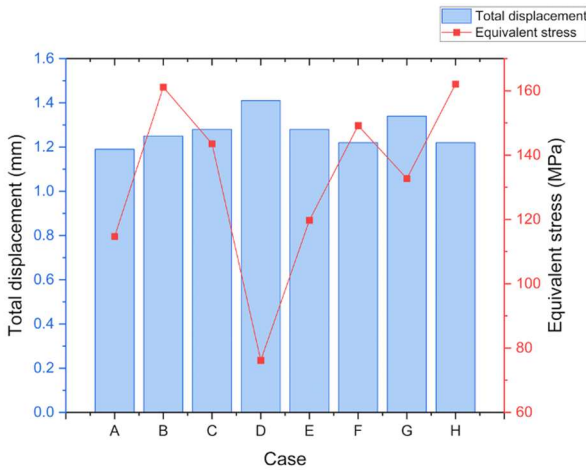


Figure 9 WAAM deformation and stress in SW simulation analysis

B. Distortion and Residual Stress Distribution of WAAM-Forging Model

Table 10 presents the effective plastic strain for the aluminium alloy process chain. A 2 mm reduction in single press showed the lowest effective plastic strain, while a 6 mm reduction in a single press resulted in the highest effective plastic strain of 0.11. Multi-press reductions showed only a small variation in maximum effective plastic strain, which ranged from 0.01 to 0.09 for the highest single-press stroke of 6 mm height reduction.

The reduction length increases the effective plastic. Longer reduction lengths enhance the effective plastic strain, leading to greater plastic deformation and refinement of the grain structure during the final forging stages. Theoretically, a higher reduction ratio increases dislocation density and energy storage, promoting the growth of precipitated phases during the process (Li et al., 2023). Figure 7 indicates that Case I and L have almost identical colour band patterns, while Cases J, K, M, and N display similar distribution patterns.

Table 10 Effective plastic strain of process chain WAAM-forging

Case	Press	Reduction length, mm	Effective plastic strain	
			Min	Max
I	Single	2	0.00	0.02
J	press	4	0.00	0.07
K		6	0.00	0.11
L	Multi	2	0.00	0.02
M	press	2, 2	0.01	0.06
N		2, 2, 2	0.01	0.09

Figure 8 illustrates the equivalent stress at 100% forming for each reduction length. As the reduction length increased by 2 mm, the stress also increases (Karunathilaka et al., 2018). Table 11 shows that Cases I and L, which have a 2 mm reduction length, exhibit the lowest equivalent stress. Single and multi-press techniques during the forging process show no

significant difference in equivalent stress. Multi-press is preferred for the actual experimental process to mitigate risk and improve strength, fatigue resistance, ductility, and fracture resistance (Manjunath et al., 2021). Future studies could explore multi-directional forging techniques for a comprehensive understanding of equivalent stress and other mechanical properties. Figure 10 provides an overall analysis of the process chain geometry in the SF simulation.

Table 11 Effective stress of process chain WAAM-forging

Case	Press	Reduction length, mm	Equivalent stress, MPa	
			Min	Max
I	Single	2	0.00	189.93
J	press	4	0.00	192.35
K		6	0.00	192.41
L	Multi	2	0.00	189.93
M	press	2, 2	0.01	191.33
N		2, 2, 2	0.01	192.41

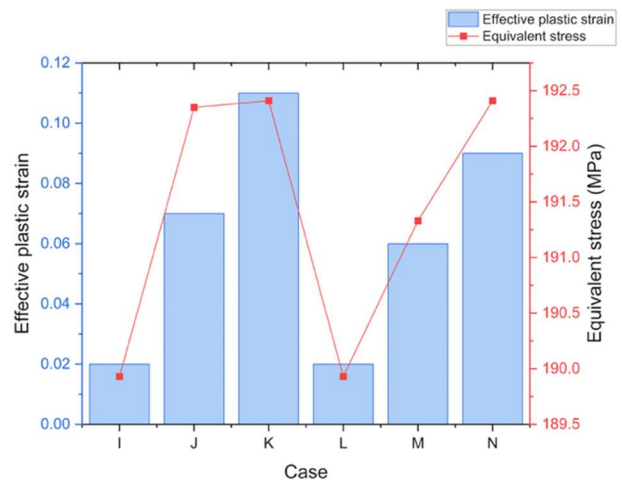


Figure 10 WAAM-Forging effective plastic strain and stress in SF simulation analysis

IV. CONCLUSION

The impact of welding and forging parameters on distortion, effective plastic strain, and residual stress in wire-arc additive manufacturing and subsequent cold forging for aluminium alloys were evaluated to improve the process integration and synergy. The findings from this study conclusively reveal several key insights. The comparison of total displacement shows that Case A exhibits the minimum displacement changes among the various strategies. The distortion in the welding zone suggests that Cases A, B, E, G, and H offer similar performance in terms of distortion. Notably, edge fixation with 2 clamps proves more effective in minimizing distortions compared to corner fixation with 4 clamps. The results demonstrate that effective plastic strain increases with the reduction length. A single press with a 2 mm reduction results in the lowest effective plastic strain, while a 6 mm reduction yields the highest strain. Multi-press reductions show only minor variations in

plastic strain, indicating that reduction length significantly impacts plastic deformation and grain structure refinement. The analysis of residual stress indicates that Case D exhibits the lowest residual stress, while Case H shows the highest. Case A, with minimal residual stress, is identified as the optimal strategy for the wire-arc additive manufacturing process, balancing residual stress distribution effectively. The findings underscore the importance of selecting appropriate fixture strategies to manage residual stress in the substrate and wall. The equivalent stress analysis reveals that a 2 mm reduction length results in the lowest equivalent stress. Although single and multi-press methods show similar stress levels, multi-press is preferred in actual experiments for its potential to enhance strength, fatigue resistance, ductility, and fracture resistance.

AUTHOR CONTRIBUTIONS

The authors confirm the equal contribution in each part of this work. All authors reviewed and approved the final version of this work. **Nornisaadila Musa** performed simulation analyses, data collection and written the manuscript. **Mohd Shahrman Adenan** developed the research framework, provided expertise in additive manufacturing, supervised the study and refined the manuscript. **Juri Saedon** assisted with simulation validation, data interpretation and manuscript revision. **Yupiter HP Manurung** contributed technical insights on wire arc simulation, validated results and reviewed the methodology. **Muhd Faiz Mat** supported the experimental setup and data collection.

ACKNOWLEDGEMENT(S)

The authors would like to acknowledge the Ministry of Higher Education (MOHE) for funding under the Geran Konsortium Kecemerlangan Penyelidikan (Hybrid Manufacturing: Integration of Direct Energy Deposition (DED) Wire-Arc Additive Manufacturing (WAAAM) With Forging Operations for Production of Netshaped Lightweight Metal Alloy Components) , 600-RMC/KKP 5/3 (003/2021) and express their gratitude to the staff member of Smart Manufacturing Research Institute (SMRI) as well as the staff of Welding Laboratory, Advanced Manufacturing Laboratory, at School of Mechanical Engineering, College of Engineering, Universiti Teknologi MARA (UiTM) Shah Alam.

REFERENCES

Altıparmak, S. C., Yardley, V. A., Shi, Z., & Lin, J. (2021). Challenges in Additive Manufacturing of High-Strength Aluminium Alloys and Current Developments in Hybrid Additive Manufacturing. *International Journal of Lightweight Materials and Manufacture*, 4(2), 246–261.

Doumenc, G., Couturier, L., Courant, B., Paillard, P., Benoit, A., Gautron, E., Girault, B., Pirling, T., Cabeza, S., & Gloaguen, D. (2022). Investigation of microstructure, hardness and residual stresses of wire and arc additive manufactured 6061 aluminium alloy.

Fu, R., Tang, S., Lu, J., Cui, Y., Li, Z., Zhang, H., Xu, T., Chen, Z., & Liu, C. (2021). Hot-Wire Arc Additive

Manufacturing of Aluminum Alloy with Reduced Porosity and High Deposition Rate. *Materials & Design*, 199, 109370.

Gokul KA, & Jose MJ. (2022). Residual Stress and Distortion in Gas Metal Arc-Based Additive Manufacturing. Retrieved from <https://ssrn.com/abstract=4294602>

Hafenecker, J., Bartels, D., Kuball, C.-M., Krefß, M., Rothfelder, R., Schmidt, M., & Merklein, M. (2023). Hybrid process chains combining metal additive manufacturing and forming – A review. *CIRP Journal of Manufacturing Science and Technology*, 46, 98–115.

Jiangang, P., Bo, Y., Jinguo, G., yu, R., hongjun, C., Liang, Z., & Hao, L. (2022). Influence of arc mode on the microstructure and mechanical properties of 5356 aluminum alloy fabricated by wire arc additive manufacturing. *Journal of Materials Research and Technology*, 20, 1893–1907.

Karunathilaka, N., Tada, N., Uemori, T., Hanamitsu, R., & Kawano, M. (2018). Effect of contact pressure applied on tool surface during cold forging on fatigue life of tool steel. *Procedia Manufacturing*, 15, 488–495

Kiran, A., Li, Y., Hodek, J., Brázda, M., Urbánek, M., & Džugan, J. (2022). Heat Source Modeling and Residual Stress Analysis for Metal Directed Energy Deposition Additive Manufacturing. *Materials*, 15(7).

Köhler, M., Fiebig, S., Hensel, J., & Dilger, K. (2019). Wire and Arc Additive Manufacturing of Aluminum Components. *MDPI Metals*, 1–9.

Li, H., Wang, L., He, W., Cheng, L., Chen, J., & Yi, L. (2023). Effect of Cold Pressing Deformation on Microstructure and Residual Stress of 7050 Aluminum Alloy Die Forgings. *Materials*, 16(14).

Manjunath, G. A., Shivakumar, S., Fernandez, R., Nikhil, R., & Sharath, P. C. (2021). A review on effect of multi-directional forging/multi-axial forging on mechanical and microstructural properties of aluminum alloy. *Materials Today: Proceedings*, 47(xxxx), 2565–2569.

Maurya, A. K., Yeom, J. T., Kang, S. W., Park, C. H., Hong, J. K., & Reddy, N. S. (2022). Optimization of Hybrid Manufacturing Process Combining Forging and Wire-Arc Additive Manufactured Ti-6Al-4V through Hot Deformation Characterization. *Journal of Alloys and Compounds*, 894.

Mohamed, M., Amer, M., Shazly, M., & Masters, I. (2021). Assessment of different ductile damage models of AA5754 for cold forming. *The International Journal of Advanced Manufacturing Technology*, 114, 1219–1231.

Napitupulu, R. A. M., Hutabarat, C., Manurung, C. S. P., Manurung, Y. H. P., & Graf, M. (2020). Comparative Study between MSC Marc/Mentat Student Version and Simufact Welding for Three-Passed Butt Joint. *IOP Conference Series: Materials Science and Engineering*, 852(1).

Rodrigues, T. A., Duarte, V., Miranda, R. M., Santos, T. G., & Oliveira, J. P. (2019). Current status and perspectives on wire and arc additive manufacturing (WAAM). *Materials*, 12(7).

Rosli, N. A., Alkahari, M. R., bin Abdollah, M. F., Maidin, S., Ramli, F. R., & Herawan, S. G. (2021). Review on effect of heat input for wire arc additive manufacturing

process. In *Journal of Materials Research and Technology* (Vol. 11, pp. 2127–2145). Elsevier Editora Ltda.

Wieczorowski, M., Pereira, A., Carou, D., Gapinski, B., & Ramírez, I. (2023). Characterization of 5356 Aluminum Walls Produced by Wire Arc Additive Manufacturing (WAAM). *Materials*, 16(7).

Xian, G., Oh, J. m., Lee, J., Cho, S. M., Yeom, J. T., Choi, Y., & Kang, N. (2022). Effect of heat input on microstructure and mechanical property of wire-arc additive manufactured Ti-6Al-4V alloy. *Welding in the World*.